arXiv:1405.3823v2 [cond-mat.mtrl-sci] 5 Jun 2015

Large-Gap Quantum Spin Hall Insulator in single layer bismuth monobromide Bi_4Br_4

Jin-Jian Zhou,[†,‡] Wanxiang Feng,[†] Cheng-Cheng Liu,[†] Shan Guan,[†] and Yugui Yao[*,†]

School of Physics, Beijing Institute of Technology, Beijing 100081, China, and Institute of Physics, Chinese Academy of Sciences and Beijing National Laboratory for Condensed Matter Physics, Beijing 100190, China

E-mail: ygyao@bit.edu.cn

Abstract

Quantum spin Hall (QSH) insulators have gapless topological edge states inside the bulk band gap, which can serve as dissipationless spin current channels. The major challenge currently is to find suitable materials for this topological state. Here, we predict a new large-gap QSH insulator with bulk direct band gap of $\sim$0.18 eV, in single-layer Bi_4Br_4, which could be exfoliated from its three-dimensional bulk material due to the weakly-bonded layered structure. The band gap of single-layer Bi_4Br_4 is tunable via strain engineering, and the QSH phase is robust against external strain. Moreover, because this material consists of special one-dimensional molecular chain as its basic building block, the single layer Bi_4Br_4 could be torn to ribbons with clean and atomically sharp edges. These nano-ribbons, which have single-Dirac-cone edge states crossing the bulk band gap, are ideal wires for dissipationless transport.

*To whom correspondence should be addressed
†Beijing Institute of Technology
‡Institute of Physics, Chinese Academy of Sciences and Beijing National Laboratory for Condensed Matter Physics

Our work thus provides a new promising material for experimental studies and practical applications of QSH effect.

KEYWORDS: Quantum spin Hall insulator, topological edge states, Bi_4Br_4, first-principles calculations.

Topological insulators (TIs) have generated a surge of interests recent years due to their rich physics and promising applications in spintronics and quantum computations.[1,2] The concept of QSH insulators, also known as two-dimensional TIs, was first proposed in graphene;[3] however, later works demonstrated that the band gap opened by spin-orbit coupling (SOC) is extremely small (10^{-3} meV) such that the QSH effect can not be observed in present experimental conditions.[4–6] Up to now, the QSH effect is only experimentally verified in HgTe/CdTe[7] and InAs/GaSb[8] quantum wells, in which stringent conditions, *e.g.* ultrahigh-quality samples and ultralow temperature, are required due to their small bulk band gaps (on the order of meV). Therefore, the search for QSH insulators with large band gaps and characteristics of easy fabrication is a key step towards the future studies and applications of QSH effect.

Many efforts have been made to search for QSH insulators with large gap and stable structures, and a number of QSH insulators have been theoretically proposed, such as silicene,[9] Bi(111) bilayer,[10] bilayers of Group III elements with Bi,[11] chemically modified Sn[12] and Bi/Sb[13] honeycomb lattices, and $ZrTe_5$/$HfTe_5$.[14] However, silicene has very small band gap, besides, an appropriate insulating substrate that can support the growth of silicene is still lacking; the Bi(111) bilayer can host sizable band gap, similar difficulty exists with the growth of the thin film material on a suitable substrate;[15,16] the chemically modified Sn, Sb and Bi honeycomb lattices are also difficult for experimental access, especially for the precise control of adatom coverage. The most promising approach for fabricating QSH insulators may be by cleaving a chemically stable two-dimensional (2D) system from their van der Waals (vdW) layered three-dimensional (3D) matrix, just like graphene made by the scotch-tape method from graphite.[17]

In this Letter, based on first-principles calculations we predict that although the 3D bulk Bi_4Br_4 is a trivial insulator, its single layer form is a QSH insulator with large-gap of $\sim$0.18 eV. The band gap can be effectively tuned by uniaxial strains, and the QSH phase is robust against external strains. The 3D bulk Bi_4Br_4 is a vdW layered semiconductor.[18] Its interlayer binding energy is comparable to other layered systems that have been successfully exfoliated, such as graphite and MoS_2. Hence, the single layer Bi_4Br_4 could be made via the mechanical exfoliation from the bulk

form. The phonon spectrum calculations further suggest that the freestanding single layer structure can be stable. Moreover, the single layer Bi_4Br_4 has one-dimensional infinite molecular chain as its building block; therefore it could be naturally torn to nano-ribbons with clean and atomically sharp edges, which are much desired for the observation of topological edge states or serving as ideal one-dimensional (1D) dissipationless conducting wires.

First-principles calculations are performed using the projector augmented wave method[19] implemented in the Vienna *ab initio* simulation package.[20] The generalized gradient approximation of Perdew-Burke-Ernzerhof (GGA-PBE) is used for the exchange correlation potential.[21] The structures are optimized employing the vdW corrections by the approach of Dion *et al.*[22,23] The experimental lattice parameters are used for the bulk system, and the same lattice parameters for single layer system (lattice constants a=13.064 Å, b=4.338 Å for Bi_4Br_4).[24,25] The ionic position are relaxed until force on each ion is less than 0.01 eV·Å^{-1}. The phonon spectrum is calculated using the PHONOPY code[26] through the DFPT approach[27] without SOC. The Maximally Localized Wannier Functions (MLWFs) for the p orbitals of Bi and Br atoms are constructed using the WANNIER90 code.[28,29] Based on the generated MLWFs, a tight-binding model for ribbons are constructed to calculate the topological edge states.

Bulk Bi_4Br_4 crystallizes in the monoclinic space group $C2/m$ (C_{2h}^3).[24,25] 1a shows the layered structure of bulk Bi_4Br_4, which can be regarded as a combined packing of the normal (marked by blue dash line) and mirror-reflected single layer along the c-axis. In each 2D layer, as shown in 1b, the basic building block is an 1D infinite molecular chain along the b-axis. 1c shows the structure of a single molecular chain. The middle Bi_{in} atoms form a zigzag chain with strongly covalent Bi_{in}-Bi_{in}bonds (∼3.0 Å), and the Br atoms are tightly attached to Bi_{ex} (∼2.9 Å) along the edges of the molecular chain. The Bi_{in}-Bi_{in} and Bi_{in}-Bi_{ex} bonds are nearly perpendicular to each other ($\alpha \sim 91^\circ$, $\beta \sim 92^\circ$). The bonds between Bi_{ex} and Br atoms in the adjacent chains [dash line in 1b] are relatively weak (∼3.6 Å). Despite the weak bonding between adjacent chains, the single-layer structure is rather stable, given that all the synthesized mixed bismuth monohalides $Bi_4Br_xI_{4-x}(x = 1,2,3)$ have the similar single-layer structure as Bi_4Br_4, while the inter-layer stacking patterns are

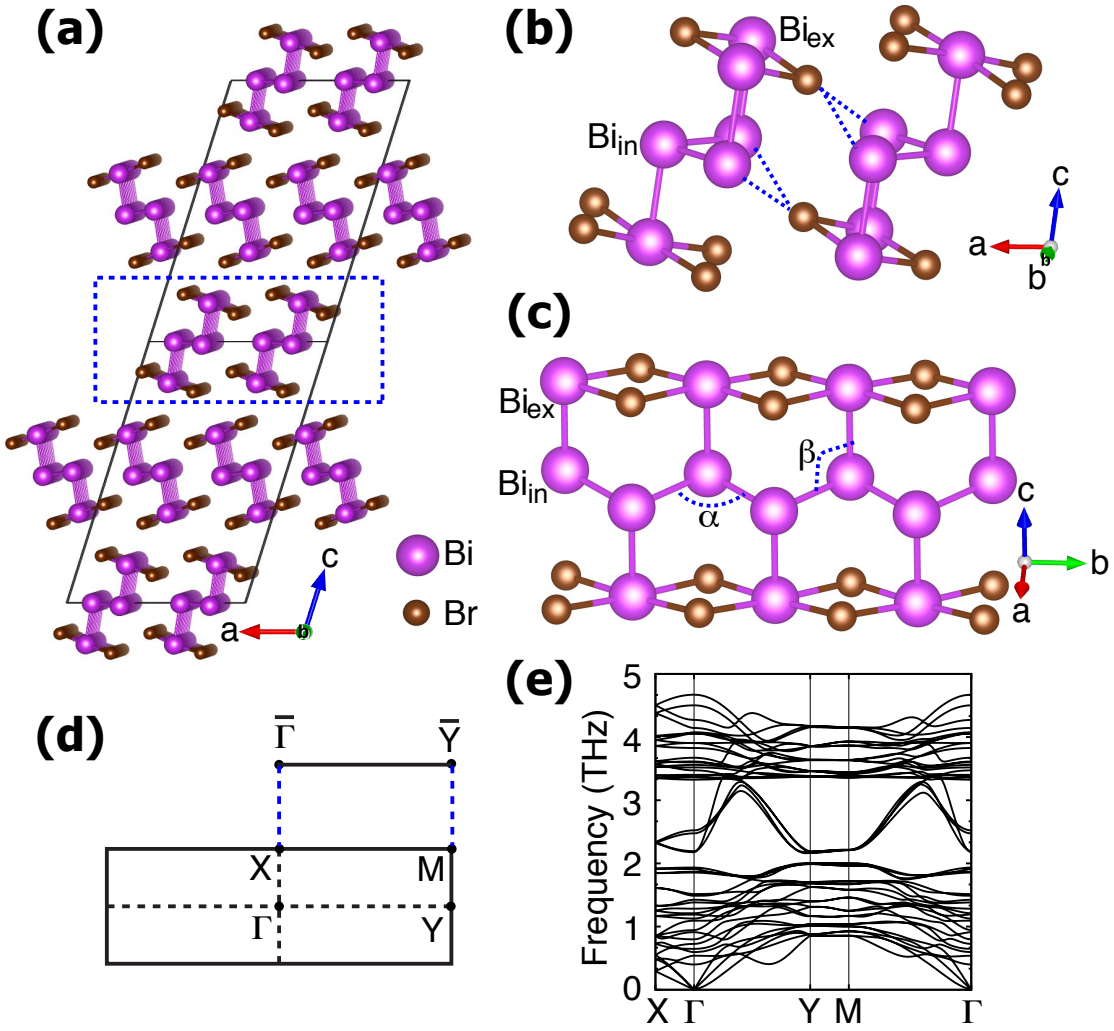

Figure 1: Crystal structure of Bi_4Br_4 in 3D (a), 2D (b), and 1D (c) representations. The large pink and small brown balls stand for Bi and Br atoms respectively. In the 1D chain, the Bi_{in} atoms in the middle form a zigzag chain, the Bi_{ex} atoms at the edge of the chain are bonded with Br atoms. (d) 2D and projected 1D Brillouin zones with high-symmetry points. (e) phonon spectrum of single layer Bi_4Br_4.

diverse.[25]

We have calculated the binding energy of the single-layer sheet to its bulk phase for Bi_4Br_4. The obtained value ($\sim$20 meV/Å^2) is in the typical range for the vdW layered compounds.[30] Specifically, the binding energy of single layer Bi_4Br_4 is comparable to the experimental result of graphene($\sim$ 12 meV/Å^2)[31] , and slightly smaller than theoretical value of MoS_2 ($\sim$26 meV/Å^2) in our calculations. This indicates that the experimental fabrication of single layer Bi_4Br_4 become possible using similar "scotch tape" method as that for graphene[17,32] or MoS_2.[33,34] The dynamic stability of single layer Bi_4Br_4 is further investigated through the phonon spectrum calculations. The calculated phonon spectrum is shown in 1e. The phonon frequencies are real at all momenta, suggesting that the single layer structure of Bi_4Br_4 is dynamically stable.

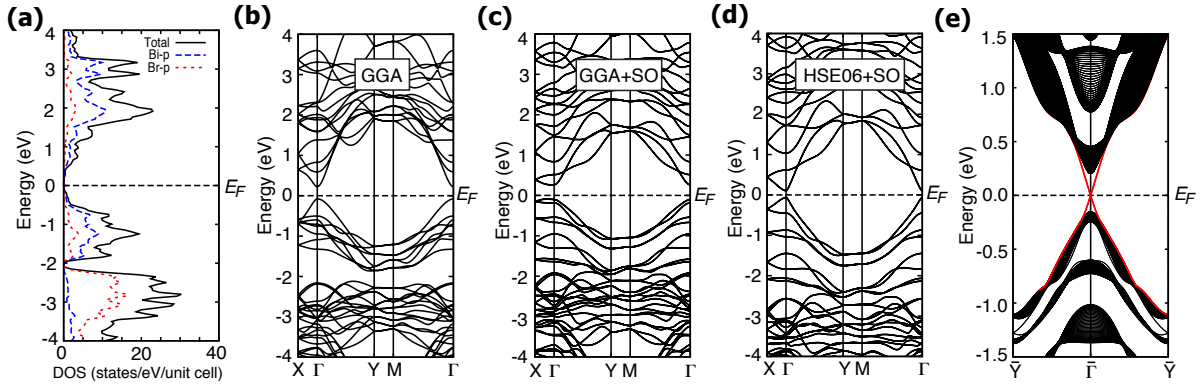

Figure 2: Density of states (a) and band structure (b) of single-layer Bi_4Br_4 without SOC. Band structures with SOC calculated by using (c) GGA and (d) HSE06 potentials. (e) Band structure of 1D nanoribbon edged along the molecular chain axis for Bi_4Br_4. Topological edge states are visualized by red lines crossing linearly at the Γ point, which indicates single-layer Bi_4Br_4 is a QSH insulator.

We now focus on the topological properties of electronic structure of single-layer Bi_4Br_4. For the convenience of discussion, hereafter all of calculations are based on a 2D conventional cell that includes two 1D chain units [see 1b]. The calculated band structure without SOC is plotted in 2b, in which one can see a direct band gap located at Γ point. From the view of density of states shown in 2a, both of the valence and conduction bands near the Fermi level are mainly constituted by Bi-6p orbitals, The states below -2 eV are dominated by Br-4p orbitals due to the larger electronegativity of Br atoms. When SOC is switched on, the band gap maintains ($\sim$0.35 eV) as shown in 2c. To

analyze the band topology, we have calculated the Z_2 topological invariant within the first-principle framework,[35] based on the parity criterion proposed by Fu and Kane.[36] The result of Z_2=1 verifies that the single layer Bi_4Br_4 is a QSH insulator. It is well known that the GGA-type calculation may produce inaccurate band gap. To further confirm the nontrivial properties of our system, we have checked the band structure of Bi_4Br_4 using the more sophisticated Heyd-Scuseria-Ernzerhof hybrid functional method (HSE06).[37] The resultant band [see 2d] has a little smaller band gap ($\sim$0.18 eV) at Γ-point compared to the GGA result, and the topological nontrivial phase remains unchanged.

The gapless chiral edge states inside the bulk band gap is the hallmark of QSH insulators. Because the coupling between the 1D molecular chains is much weaker than the intra-chain bonding,[18] a natural nanoribbon can be constructed along the *b*-axis without any dangling bond. With the nanoribbon width of 40 chains ($\approx$26 nm), the calculated band structure is presented in 2e. One can see explicitly that the gapless edge states appear in bulk band gap cross linearly at the Γ point. The Fermi velocity of edge states in single layer Bi_4Br_4 is $\sim 4.8\times10^5$ m/s, which is slightly smaller than that of 5.5×10^5 m/s in HgTe/CdTe quantum well,[2] but is remarkably larger than that of 3×10^4 m/s in InAs/GaSb quantum well.[8] This high Fermi velocity is beneficial to the fabrication of high-speed spintronics devices.

To elucidate the physical mechanism of the band inversion, we study the band structure evolution at Γ point, starting from the atomic orbitals. The schematic diagram of the evolution is plotted in 3a. The 2D single layer Bi_4Br_4 cell consists of two 1D chains, and each chain has four Bi atoms and four Br atoms in a unit-cell. The Br-4p orbitals stay deep below the Fermi level due to the much larger electronegativity of Bromine. Therefore, it is reasonable to neglect the Br atoms, and only consider the Bi-6p orbitals. For clarity, the simplified structure with only Bi atoms is schematically plotted in 3b.

We first consider the strongly covalent bonds within the 1D chain, and then take into account the weak inter-chain couping. For the 1D chain, the Bloch orbital at Γ point is given by $|p_\alpha\rangle = \sum_i p^i_\alpha$, where p^i_α ($\alpha = x,y,z$) are the atomic orbitals in unit-cell R_i. At stage (1), mirror symmetry is

considered. The structure has mirror symmetry with mirror plane parallel to xz plane. The $p_{x/z}$ and p_y orbitals at Γ point have different parities under mirror operation, hence they will not mix with each other (when SOC is absent). The p_y orbital has higher energy because of the much stronger σ-type hopping between p_y^i and p_y^{i+1} compared to the π-type of $p_{x/z}$. At stage (2), the inversion symmetry of the chain is considered. Under inversion operation, the two Bi_{in} (Bi_{ex}) atoms interchange site with each other. Orbitals from these two atoms can be combined to form bonding and anti-bonding states with splitted levels, which are given by

$$|Bi_{in/ex}, \alpha^{\pm}\rangle = \frac{1}{\sqrt{2}}(|Bi^1_{in/ex}, \alpha\rangle \mp |Bi^2_{in/ex}, \alpha\rangle)$$

with $\alpha = p_x, p_y, p_z$. They have definite parities as denoted in the upper index $\pm$. Only those states with the same parity can further couple with each other. We discuss the intra-chain bonding induced coupling between those states as following: (1) The splitting energy ΔE_x between $|\mathrm{Bi}_{in}, p_x^+\rangle$ and $|\mathrm{Bi}_{in}, p_x^-\rangle$ is quite large due to the short Bi_{in}-Bi_{in} bond length, so does the $|\mathrm{Bi}_{in}, p_y^{\pm}\rangle$. In addition, the relative size of ΔE_x and ΔE_y depends on the angle θ [see 3b]. The $p_x(p_y)$ orbital hopping t_{xx} (t_{yy}) between the two Bi_{in} atoms, which determine the ΔE_x (ΔE_y), is related to θ, namely, t_{xx} (t_{yy}) can be given by $t_{pp\sigma}\sin\theta^2 + t_{pp\pi}\cos\theta^2$ ($t_{pp\sigma}\cos\theta^2 + t_{pp\pi}\sin\theta^2$). Therefore, the reduction of θ will decrease the ΔE_x and increase the ΔE_y. (2) The orbital hopping between the two Bi_{ex} atoms, which locate at different sides of the chain, is negligible. However, $|\mathrm{Bi}_{ex}, p_{x/y}^{\pm}\rangle$ can be coupled to $|\mathrm{Bi}_{in}, p_{x/y}^{\pm}\rangle$ through the $\pi-$bonding of $p_{x/y}$ orbital between Bi_{in}-Bi_{ex} atoms, which shifts $|\mathrm{Bi}_{ex}, p_{x/y}^+\rangle$ upward and $|\mathrm{Bi}_{ex}, p_{x/y}^-\rangle$ downward. (3) Due to the strong $\sigma-$bonding of p_z orbital between Bi_{in}-Bi_{ex} atoms, $|\mathrm{Bi}_{ex}, p_z^{\pm}\rangle$ mix with $|\mathrm{Bi}_{in}, p_z^{\pm}\rangle$ and splits into $|\mathrm{B1}, p_z^{\pm}\rangle$ and $|\mathrm{B2}, p_z^{\pm}\rangle$ states.

So far, we have considered all the intra-chain bonding. At stage (3), we start to count in the inter-chain coupling. The inter-chain coupling is dominated by the hopping between p_x orbitals because their orientations are parallel to the inter-chain direction. The $p_x^{\pm}$ orbitals from two adjacent chains (labeled as A, B) within the 2D cell are further splitted into bonding and anti-bonding

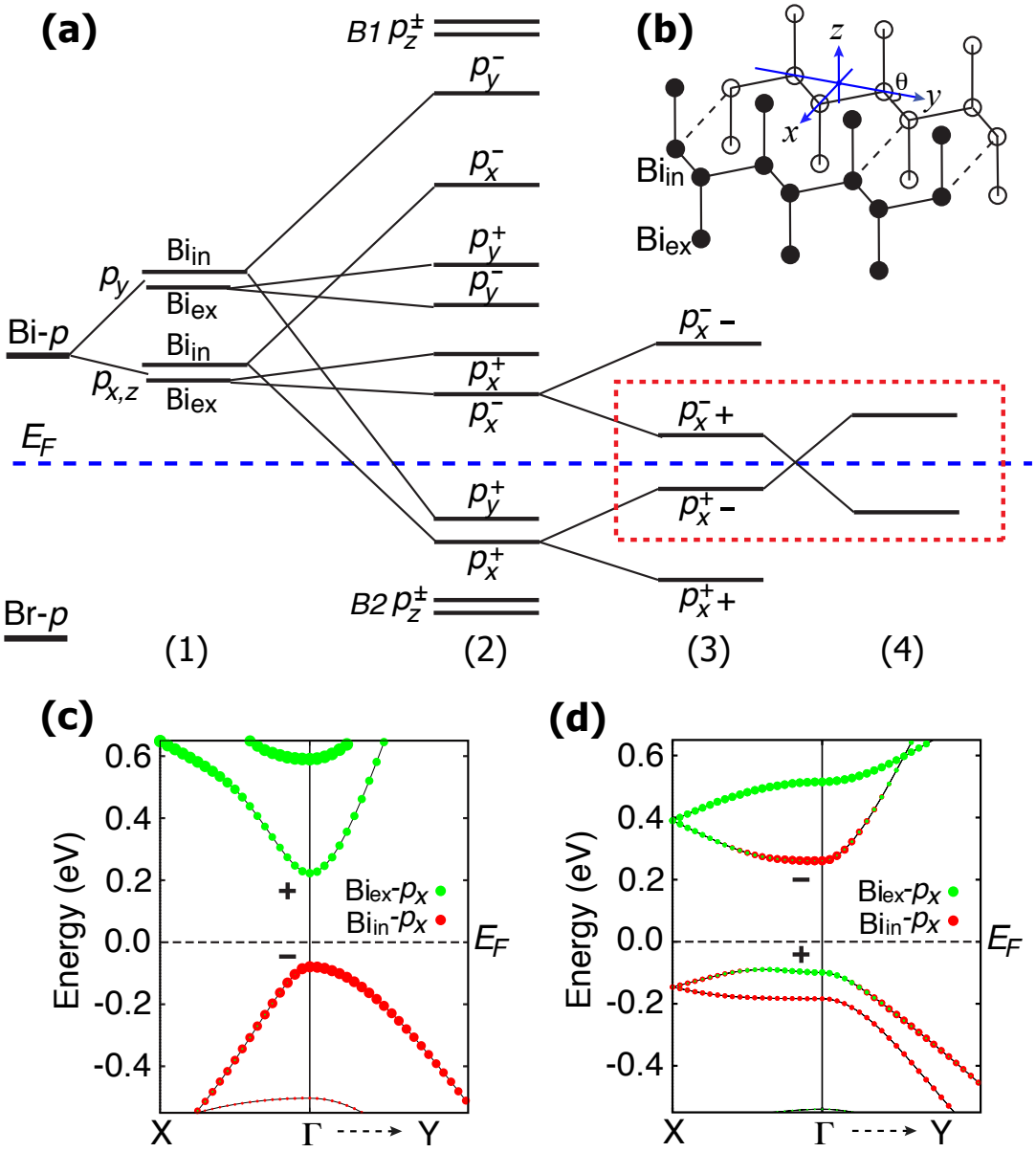

Figure 3: (a) Schematic diagram of the band evolution at Γ-point. The evolution stages are explained in the main text. (b) Schematic figure of the single layer Bi_4Br_4 structure with Br-atoms neglected. The filled and empty circles stand for Bi-atoms from adjacent chains. The solid lines denote strong intra-chain bonds, the dash lines denote weak inter-chain coupling. The Bi_{in}-p_x and Bi_{ex}-p_x orbital projected character of bands without (c) and with (d) SOC, the parity is labeled for CBM and VBM at Γ-point.

states, for example

$$|Bi_{in/ex}, p_x^+, \pm\rangle = \frac{1}{\sqrt{2}}(|Bi_{in/ex}^A, p_x^+\rangle \mp |Bi_{in/ex}^B, p_x^+\rangle)$$

At final stage (4), the SOC is considered. The SOC mixes the orbital and spin with total angular momentum conserved, which results in the level repulsion between $|\mathrm{Bi}_{in/ex}, p_x^{\pm}\rangle$ and $|\mathrm{Bi}_{in/ex}, p_y^{\pm}\rangle$,[38] thus push the $|\mathrm{Bi}_{ex}, p_x^-, +\rangle$ downward and the $|\mathrm{Bi}_{in}, p_x^+, -\rangle$ upward, as shown in 3a. Consequently, the band order is inverted (marked by the red dashed box). We show the Bi_{in}-p_x and Bi_{ex}-p_x orbitals projected bands in 3c (without SOC) and 3d (with SOC). As we can seen, in the absence of SOC, the valence band maximum(VBM) is dominated by the Bi_{in}-p_x orbital with negative parity, while the conduction band minimum (CBM) is dominated by the Bi_{ex}-p_x orbital with positive parity. After SOC is turned on, both the orbital character and the parity of CBM and VBM are inverted.

Application of external strain can effectively modify the band gap of single layer Bi_4Br_4, as shown in 4. Due to the structural anisotropy, we adopt separately the uniaxial strains along *a*- and *b*-axises. The change of band gap under the uniaxial strains displays a opposite behavior, i.e. increasing the lattice constant *a* will diminish the band gap, while increasing the lattice constant *b* will enlarge the band gap. This behavior can be understood from the above band evolution analysis. Increasing *a* will extend the inter-chain distance, which decreases the inter-chain coupling. The weakened inter-chain coupling will diminish the splitting at stage (3) in 3a and decrease the band gap ultimately. As we increase the lattice constant *b*, the angle θ becomes smaller accordingly while the Bi_{in}-Bi_{in} bond length hardly changes. With smaller θ, the $|\mathrm{Bi}_{in}, p_x^+\rangle$ will move upward to reduce the splitting [stage (2) in 3a], which then enlarges the band gap ultimately.

Although the band gap is tunable via strain engineering, the topological nontrivial phase of single layer Bi_4Br_4 survives in a large range of strains from $\sim$ -6% to 6%. Hence, the QSH phase can be robust against lattice mismatch strain when the single layer Bi_4Br_4 is supported by a substrate. We have also investigated another bismuth monohalides Bi_4I_4, which has the similar

structure as Bi_4Br_4.[24,25] The single layer Bi_4I_4 is near the boundary of topological trivial and nontrivial phase transition[see 4]; hence its QSH phase can be effectively tuned by uniaxial strains.

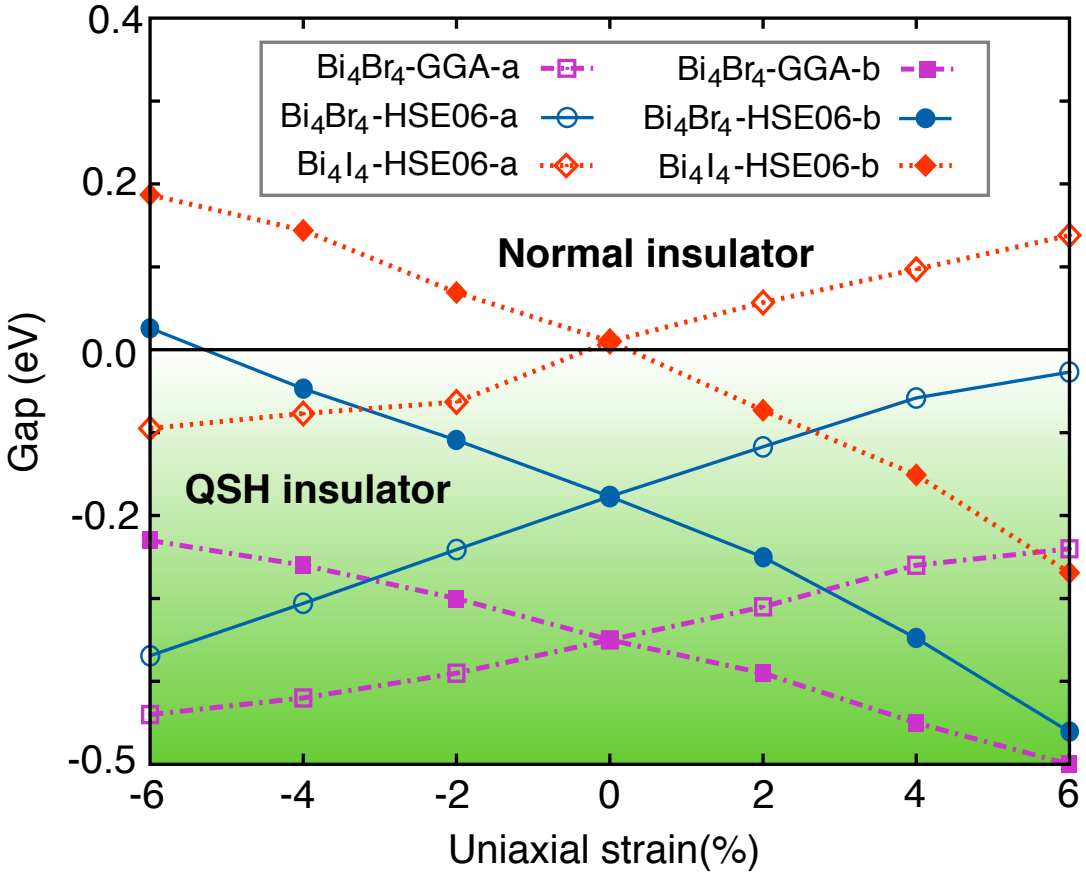

Figure 4: Band gaps as a function of uniaxial strains. The negative band gaps indicate non-trivial topological phases. The uniaxial strains along a- and b-axises are adopted separately. Band gaps of single layer Bi_4Br_4 calculated by using GGA-PBE and HSE06 potentials, and band gaps of single layer Bi_4I_4 calculated by using HSE06 potential are presented respectively.

Finally, we extend our discussion to the multilayer structures of Bi_4Br_4. Usually, when the single-layers are stacked together to form a multilayer film or 3D compound, the band gap will be reduced due to the inter-layer orbital hopping. In our systems, the inter-layer coupling is rather weak and the band edges are all dominated by the in-plane orbitals; therefore, we do not expect much band gap reduction in multilayer Bi_4Br_4 compared to the single layer one. Even for the 3D compound, the inverted band gap ($\sim$0.15 eV) is only reduced by $\sim$30 meV according to our HSE06 calculations. Within the weak coupling limit, the multilayer Bi_4Br_4 with even (odd) number of

layers would have even (odd) times of band inversions at Γ points.[39] Therefore, the Z_2 topological invariant would exhibit an interesting even-odd oscillation with increasing number of layers. The 3D bulk Bi_4Br_4, which contains two layers in one unit cell, is a trivial insulator, while the ultra-thin films with odd number of layers are QSH insulators.[39]

In summary, the 2D Bi_4Br_4 is a promising QSH insulator with large band gap ($\sim$0.18 eV), while the single layer Bi_4I_4 is near the boundary of topological trivial and nontrivial phase transition. Due to the highly structural anisotropy, natural Bi_4Br_4 nonaribbons can be constructed without any dangling bond. These nanoribbons, which have single-Dirac-cone topological edge states inside the bulk band gap, can serve as ideal 1D wires for dissipationless transport, or be utilized to create and manipulate majorana fermion via, e.g. putting the nanoribbon on the s-wave superconductors with external magnetic fields.[40]

Acknowledgement

This work was supported by the MOST Project of China (Nos. 2014CB920903, 2013CB921903, 2011CBA00100), the NSF of China (Nos. 11174337, 11225418, 11374033) and the SRFDPHE of China (No. 20121101110046, 20131101120052).

References

(1) Hasan, M. Z.; Kane, C. L. *Rev. Mod. Phys.* **2010**, *82*, 3045–3067.

(2) Qi, X.-L.; Zhang, S.-C. *Rev. Mod. Phys.* **2011**, *83*, 1057–1110.

(3) Kane, C. L.; Mele, E. J. *Phys. Rev. Lett.* **2005**, *95*, 226801.

(4) Yao, Y.; Ye, F.; Qi, X.-L.; Zhang, S.-C.; Fang, Z. *Phys. Rev. B* **2007**, *75*, 041401.

(5) Huertas-Hernando, D.; Guinea, F.; Brataas, A. *Phys. Rev. B* **2006**, *74*, 155426.

(6) Min, H.; Hill, J. E.; Sinitsyn, N. A.; Sahu, B. R.; Kleinman, L.; MacDonald, A. H. *Phys. Rev. B* **2006**, *74*, 165310.

(7) KÃűnig, M.; Wiedmann, S.; BrÃijne, C.; Roth, A.; Buhmann, H.; Molenkamp, L. W.; Qi, X.-L.; Zhang, S.-C. *Science* **2007**, *318*, 766–770.

(8) Knez, I.; Du, R.-R.; Sullivan, G. *Phys. Rev. Lett.* **2011**, *107*, 136603.

(9) (a) Liu, C.-C.; Feng, W.; Yao, Y. *Phys. Rev. Lett.* **2011**, *107*, 076802; (b) Liu, C.-C.; Jiang, H.; Yao, Y. *Phys. Rev. B* **2011**, *84*, 195430.

(10) Murakami, S. *Phys. Rev. Lett.* **2006**, *97*, 236805.

(11) Chuang, F.-C.; Yao, L.-Z.; Huang, Z.-Q.; Liu, Y.-T.; Hsu, C.-H.; Das, T.; Lin, H.; Bansil, A. *Nano Lett.* **2014**, *14*, 2505–2508.

(12) Xu, Y.; Yan, B.; Zhang, H.-J.; Wang, J.; Xu, G.; Tang, P.; Duan, W.; Zhang, S.-C. *Phys. Rev. Lett.* **2013**, *111*, 136804.

(13) (a) Song, Z.; Liu, C.-C.; Yang, J.; Han, J.; Ye, M.; Fu, B.; Yang, Y.; Niu, Q.; Lu, J.; Yao, Y. *arXiv:1402.2399* **2014**, ; (b) Liu, C.-C.; Guan, S.; Song, Z.; Yang, S. A.; Yang, J.; Yao, Y. *arXiv:1402.5817* **2014**,

(14) Weng, H.; Dai, X.; Fang, Z. *Phys. Rev. X* **2014**, *4*, 011002.

(15) Hirahara, T.; Bihlmayer, G.; Sakamoto, Y.; Yamada, M.; Miyazaki, H.; Kimura, S.-i.; Blügel, S.; Hasegawa, S. *Phys. Rev. Lett.* **2011**, *107*, 166801.

(16) Yang, F. et al. *Phys. Rev. Lett.* **2012**, *109*, 016801.

(17) Novoselov, K. S.; Geim, A. K.; Morozov, S. V.; Jiang, D.; Zhang, Y.; Dubonos, S. V.; Grigorieva, I. V.; Firsov, A. A. *Science* **2004**, *306*, 666–669.

(18) Filatova, T. G.; Gurin, P. V.; Kloo, L.; Kulbachinskii, V. A.; Kuznetsov, A. N.; Kytin, V. G.; Lindsjo, M.; Popovkin, B. A. *J. Solid State Chem.* **2007**, *180*, 1103–1109.

(19) Blochl, P. E. *Phys. Rev. B* **1994**, *50*, 17953–17979.

(20) (a) Kresse, G.; Hafner, J. *Phys. Rev. B* **1993**, *47*, 558–561; (b) Kresse, G.; Furthmüller, J. *Phys. Rev. B* **1996**, *54*, 11169–11186.

(21) Perdew, J. P.; Burke, K.; Ernzerhof, M. *Phys. Rev. Lett.* **1996**, *77*, 3865–3868.

(22) Klimeš, J.; Bowler, D. R.; Michaelides, A. *Phys. Rev. B* **2011**, *83*, 195131.

(23) Dion, M.; Rydberg, H.; Schröder, E.; Langreth, D. C.; Lundqvist, B. I. *Phys. Rev. Lett.* **2004**, *92*, 246401.

(24) von Benda, H.; Simon, A.; Bauhofer, W. *Z. Anorg. Allg. Chem.* **1978**, *438*, 53–67.

(25) Dikarev, E. V.; Popovkin, B. A.; Shevelkov, A. V. *Russ. Chem. Bull. Int. Ed.* **2001**, *50*, 2304–2309.

(26) Togo, A.; Oba, F.; Tanaka, I. *Phys. Rev. B* **2008**, *78*, 134106.

(27) Gonze, X.; Lee, C. *Phys. Rev. B* **1997**, *55*, 10355–10368.

(28) (a) Marzari, N.; Vanderbilt, D. *Phys. Rev. B* **1997**, *56*, 12847–12865; (b) Souza, I.; Marzari, N.; Vanderbilt, D. *Phys. Rev. B* **2001**, *65*, 035109.

(29) Mostofi, A. A.; Yates, J. R.; Lee, Y.-S.; Souza, I.; Vanderbilt, D.; Marzari, N. *Comput. Phys. Commun.* **2008**, *178*, 685 – 699.

(30) Björkman, T.; Gulans, A.; Krasheninnikov, A. V.; Nieminen, R. M. *Phys. Rev. Lett.* **2012**, *108*, 235502.

(31) Liu, Z.; Liu, J. Z.; Cheng, Y.; Li, Z.; Wang, L.; Zheng, Q. *Phys. Rev. B* **2012**, *85*, 205418.

(32) Geim, A. K.; Novoselov, K. S. *Nat. Mater.* **2007**, *6*, 183–191.

(33) Novoselov, K. S.; Jiang, D.; Schedin, F.; Booth, T. J.; Khotkevich, V. V.; Morozov, S. V.; Geim, A. K. *Proc. Natl. Acad. Sci. U.S.A.* **2005**, *102*, 10451–10453.

(34) Radisavljevic, B.; Radenovic, A.; Brivio, J.; Giacometti, V.; Kis, A. *Nat. Nanotech.* **2011**, *6*, 147–150.

(35) Feng, W.; Wen, J.; Zhou, J.; Xiao, D.; Yao, Y. *Comput. Phys. Commun.* **2012**, *183*, 1849 – 1859.

(36) Fu, L.; Kane, C. L. *Phys. Rev. B* **2007**, *76*, 045302.

(37) Heyd, J.; Scuseria, G. E.; Ernzerhof, M. *J. Chem. Phys.* **2003**, *118*, 8207–8215.

(38) Liu, C.-X.; Qi, X.-L.; Zhang, H.; Dai, X.; Fang, Z.; Zhang, S.-C. *Phys. Rev. B* **2010**, *82*, 045122.

(39) Yan, B.; Müchler, L.; Felser, C. *Phys. Rev. Lett.* **2012**, *109*, 116406.

(40) Alicea, J. *Rep. Prog. Phys.* **2012**, *75*, 076501.

Graphical TOC Entry